# Geometric Parameter Effects on Ensemble Contributions to Catalysis: $H_2O_2$ Formation from $H_2$ and $O_2$ on AuPd Alloys. A First Principles Study

**Hyung Chul Ham,[†] Gyeong S. Hwang,*[,†] Jonghee Han,[‡] Suk Woo Nam,[‡] and Tae Hoon Lim[‡]**

*Department of Chemical Engineering, University of Texas at Austin, Austin, Texas 78712, and Center for Fuel Cell Research, Korea Institute of Science and Technology, Seoul, Korea*

*Received: March 30, 2010; Revised Manuscript Received: July 21, 2010*

Using first principles calculations, we examine how the ensemble effect on the performance of bimetallic catalysts is affected by the change of surface electronic structure associated with their geometric parameters. We look at $H_2O_2$ formation from $H_2$ and $O_2$ based on three different Pd monomer systems including AuPd adlayers with a Pd monomer each on Pd(111) [$AuPd_M$/Pd(111)] and Au(111) [$AuPd_M$/Au(111)] and a 55-atom cluster with $Au_{41}Pd$ shell and $Pd_{13}$ core [$Au_{41}Pd@Pd_{13}$]. Our calculations show that $H_2O_2$ selectivity tends to be significantly deteriorated in the $Au_{41}Pd@Pd_{13}$ and $AuPd_M$/Au(111) cases, as compared to the $AuPd_M$/Pd(111) case. This is largely due to enhancement of the activity of corresponding surface Pd and its Au neighbors, while isolated Pd surface sites surrounded by less active Au are responsible for the $H_2O_2$ formation by suppressing O−O cleavage. This study highlights that ensemble contributions in multimetallic nanocatalysts can be a strong function of their geometric conditions, particularly local strain and effective atomic coordination number at the surface, that are directly related to surface electronic states.

## 1. Introduction

The efficiency of bimetallic gold−palladium (AuPd) catalysts has been found to be notably enhanced compared to monometallic Pd and Au catalysts in various reactions including direct synthesis of hydrogen peroxide ($H_2O_2$) from hydrogen ($H_2$) and oxygen ($O_2$)[1,2] and production of vinyl acetate monomer.[3−6] Recent studies have provided evidence that the surface reactivity of bimetallic alloys is to a large extent governed by creation of unique mixed-metal surface sites [the so-called ensemble (geometric) effect[7]] and electronic state change by metal−metal interactions [the so-called ligand (electronic) effect]. In addition, the activity of metal catalysts can be modified by the presence of low-coordination surface atoms and the stress imposed on the outer-layer atoms, in association with the size and shape of nanoparticle catalysts and the lattice parameter difference between the substrate and the adlayer. However, the quantitative assessment of the relative roles of these effects has not yet been made, largely due to difficulty in direct characterization.

A recent first principles study[8] demonstrated that the selectivity of $H_2O_2$ in direct oxidation of $H_2$ is a strong function of the arrangement of Pd and Au surface atoms in AuPd alloy catalysts. In particular, isolated Pd monomers surrounded by less active Au atoms are primarily responsible for the significantly enhanced $H_2O_2$ selectivity by suppressing O−O bond cleavage. It has also been reported that Pd monomers play a significant role in enhancing the catalytic activity for hydrogen evolution,[9] vinyl acetate synthesis,[4] and carbon monoxide adsorption and oxidation.[6] The ensemble effect is apparently attributed to the large activity difference between Pd and Au. However, for a given ensemble the relative chemical activity of constituent surface atoms can be altered by the change of geometric parameters and consequent surface electronic states. Therefore, it will be instructive to examine how the change of surface electronic structure affects the ensemble effect in alloy catalysts.

In this study, we attempt to understand the interplay between the ensemble and electronic contributions associated with changes in the geometric parameters. We consider three different Pd monomer systems in the slab and cluster geometries: $AuPd_M$/Pd(111), $AuPd_M$/Au(111), and $Au_{41}Pd@Pd_{13}$. Using density functional theory calculations, we first look at how the electronic state of Au and Pd surface atoms changes with varying geometric conditions and then examine how the electronic state change affects the activity and selectivity toward direct $H_2O_2$ synthesis from $H_2$ and $O_2$. The improved understanding will assist in rationally designing bimetallic nanocatalysts.

## 2. Computational Method

The calculations reported herein were performed on the basis of spin-polarized density functional theory (DFT) within the generalized gradient approximation (GGA-PW91[10]), as implemented in the Vienna Ab-initio Simulation Package (VASP).[11] The projector augmented wave (PAW) method with a plane-wave basis set was employed to describe the interaction between ion cores and valence electrons.[12] The PAW method is in principle an all-electron frozen-core approach that considers exact valence wave functions. Valence configurations employed are $5d^{10}6s^1$ for Au, $4d^9 5s^1$ for Pd, and $2s^2 2p^4$ for O. An energy cutoff of 350 eV was applied for the plane-wave expansion of the electronic eigenfunctions. Reaction pathways and barriers were determined using the climbing-image nudged elastic band method (*c*-NEBM) with eight intermediate images for each elementary step.[13]

In this work, as illustrated in Figure 1, we considered three different Pd monomer systems: (a) $AuPd_M$/Pd(111) in which the surface Au layer with a Pd monomer is overlaid on a Pd(111) slab; (b) $AuPd_M$/Au(111) in which the $AuPd_M$ layer is on a Au(111) slab; and (c) $Au_{41}Pd@Pd_{13}$ which refers to a 55-atom icosahedral cluster with a 13-atom Pd core and an Au shell that

* To whom correspondence should be addressed: Ph 512-471-4847; Fax 512-471-7060; e-mail gshwang@che.utexas.edu.
[†] University of Texas at Austin.
[‡] Korea Institute of Science and Technology.

10.1021/jp102851d 
Published on Web 08/19/2010

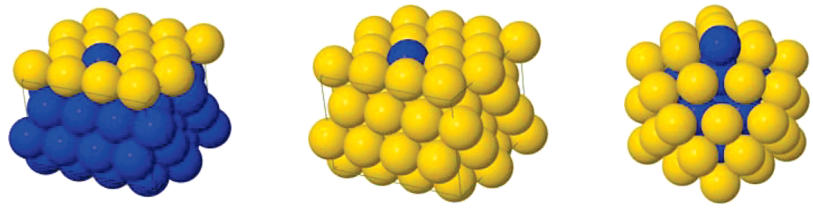


**Figure 1.** Model AuPd alloy surfaces considered each of which contains a Pd monomer. (a) $AuPd_M/Pd(111)$ where the surface Au layer with a Pd monomer is overlaid on a Pd(111) slab, (b) $AuPd_M/Au(111)$ where the $AuPd_M$ layer is on a Au(111) slab, and (c) $Au_{41}Pd@Pd_{13}$ which has a 13-atom Pd core and an Au shell with a Pd monomer at the lowest energy position. The black (blue) and gray (gold) balls represent Pd and Au atoms, respectively.

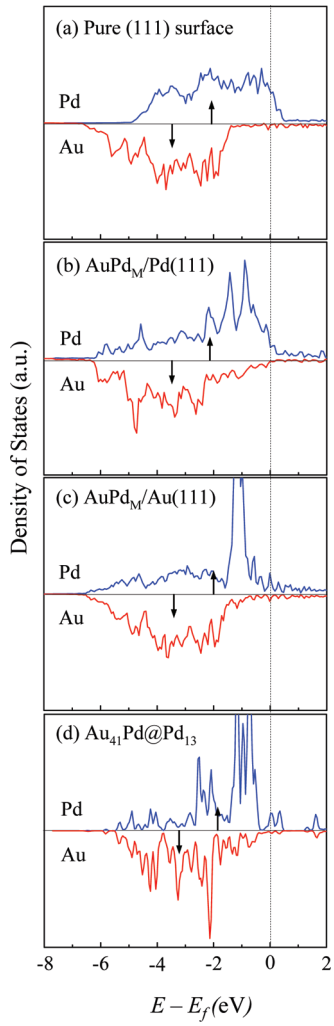


**Figure 2.** Density of states (DOS) project onto the outmost d states of the Pd monomers (4d) and adjacent Au (5d) surface atoms in (b) $AuPd_M/Pd(111)$, (c) $AuPd_M/Au(111)$, and (d) $Au_{41}Pd_M@Pd_{13}$, together with (a) pure (111) surface atoms for comparison. The dotted line indicates the Fermi level position, and d-band center positions are also indicated by arrows.

contains a Pd monomer at the lowest-energy site (more details are available in Supporting Information). For the $AuPd_M/Pd(111)$ (Figure 1a) and $AuPd_M/Au(111)$ (Figure 1b) cases, the supercell slab consists of a rectangular $2\sqrt{3} \times 4$ surface unit cell with four atomic layers; each layer contains 16 atoms. The slab is separated from its periodic images in the vertical direction by a vacuum space corresponding to seven atomic layers. The bottom two layers were fixed at corresponding bulk positions, and the upper two layers were fully relaxed using the conjugate gradient method until residual forces on all the constituent atoms

**TABLE 1: Calculated d-Band Centers ($\varepsilon_d$ in eV) of Pd and Adjacent Au Surface Atoms and Distances ($d_{Pd-X}$ in Å) of Pd−Pd [in Pd(111)] and Pd−Au [in the Others]**

| | $d_{Pd-X(X=Pd\ or\ Au)}$ | $\varepsilon_d$(Pd) | $\varepsilon_d$(Au) |
|---|---|---|---|
| Pd(111) or Au(111) | 2.80 | −2.06 | −3.53 |
| $AuPd_M/Pd(111)$ | 2.78 | −2.17 | −3.54 |
| $AuPd_M/Au(111)$ | 2.93 | −2.01 | −3.44 |
| $Au_{41}Pd@Pd_{13}$ | 2.79 | −1.88 | −3.18 |

become smaller than $5 \times 10^{-2}$ eV/Å. All atoms in the $Au_{41}Pd@Pd_{13}$ cluster (Figure 1c) were fully relaxed with the same force−convergence criterion. For Brillouin zone integration in the slab systems, we used a $(2 \times 2 \times 1)$ Monkhorst−Pack mesh of k points to determine the optimal geometries and total energies, and increased the k-point mesh size up to $(7 \times 7 \times 1)$ to refine corresponding electronic structures. For the cluster system, one k-point (Gamma point) was employed for Brillouin zone integration, while the $Au_{41}Pd@Pd_{13}$ cluster was placed in a periodic cubic box of dimension = 25 Å × 25 Å × 25 Å. The lattice constants for bulk Pd and Au were predicted to be 3.95 and 4.18 Å, virtually identical to previous DFT-GGA calculations[14,15] and also in good agreement with respective experimental values of 3.89 and 4.08 Å. We further checked the convergence of our calculation results with respect to k-point mesh size, cutoff energy, and vacuum space, which suggests that the chosen values are sufficient for describing the surface chemistry of the model systems considered.

## 3. Results and Discussion

**Surface Electronic States.** We looked at variations in the electronic states of Pd monomer and its nearest Au neighbors for the three $AuPd_M$ surface alloys considered. Figure 2 shows the d-projected density of states (DOS) of surface Pd (4d) and neighboring Au (5d) atoms, together with pure Pd(111) and Au(111) surfaces for comparison. The change of d-electron distributions could be described in a somewhat quantitative manner by the shift of corresponding d-band centers. Previous studies[7,16,17] suggested that the average energy of the d-band could be used as a general measure of local surface reactivity; i.e., an upshift of the d-band center toward the Fermi level is expected to imply enhancement in the surface chemical reactivity, and vice versa. Table 1 summarizes the computed d-band centers of the surface Pd and Au atoms.

For the $AuPd_M/Pd(111)$ case (b), the d states of the surface Pd and neighboring Au atoms are somewhat broadened relative to pure Pd(111) and Au(111) (a), implying the effective interaction among the Pd monomer and Au neighbors. The Pd d-band center is located at −2.17 eV, which is lower than −2.06 eV for clean Pd(111), while there is no noticeable shift in the Au d-band center [$\varepsilon_d$ = −3.54 eV as compared to −3.53 eV for clean Au(111)].

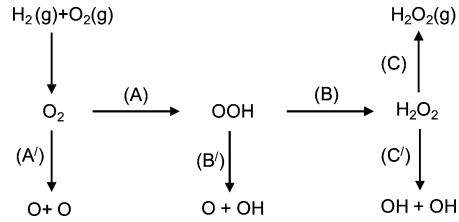


**Figure 3.** Schematic illustration of $H_2O_2$ formation and competing decomposition steps considered in this study: (A) $O_2$ hydrogenation, (A)′ O + O scission, (B) OOH hydrogenation, (B)′ O + OH scission, (C) $H_2O_2$ desorption, (C)′ OH + OH scission.

For the $AuPd_M$/Au(111) case (c), the d states of the Pd monomer and its Au surface neighbors exhibit narrower distributions compared to the $AuPd_M$/Pd(111) case. In addition, both Pd and Au d-band centers move upward in energy, i.e., from −2.17 to −2.01 eV and from −3.54 to −3.44 eV, respectively. The d-bandwidth narrowing and upshift may indicate enhanced chemical activity for the surface Pd and Au atoms. This can be associated with the tensily strained surface where the Pd−Au distance is increased to 2.93 Å [$AuPd_M$/Au(111)] compared to 2.78 Å for the $AuPd_M$/Pd(111) case; note that the Pd−Pd distance is predicted to be 2.80 Å on clean Pd(111). The correlation between surface strain and chemical activity has also been evidenced by a series of earlier experimental and theoretical studies.[18,19]

For the $Au_{41}Pd@Pd_{13}$ case (d), our calculation shows a substantial upshift in the d-band centers of the outer-shell Pd ($\varepsilon_d = -1.88$ eV) and adjacent Au ($\varepsilon_d = -3.18$ eV) atoms as compared to the $AuPd_M$/Au(111) and $AuPd_M$/Au(111) cases. This implies chemical activity enhancement of the skin surface Pd and Au atoms, which is apparently associated with their reduced coordination number and inherent mechanical strain created in the small cluster.

**$H_2O_2$ Formation from $H_2$ and $O_2$.** We examined how the electronic state change of the surface Pd monomer and

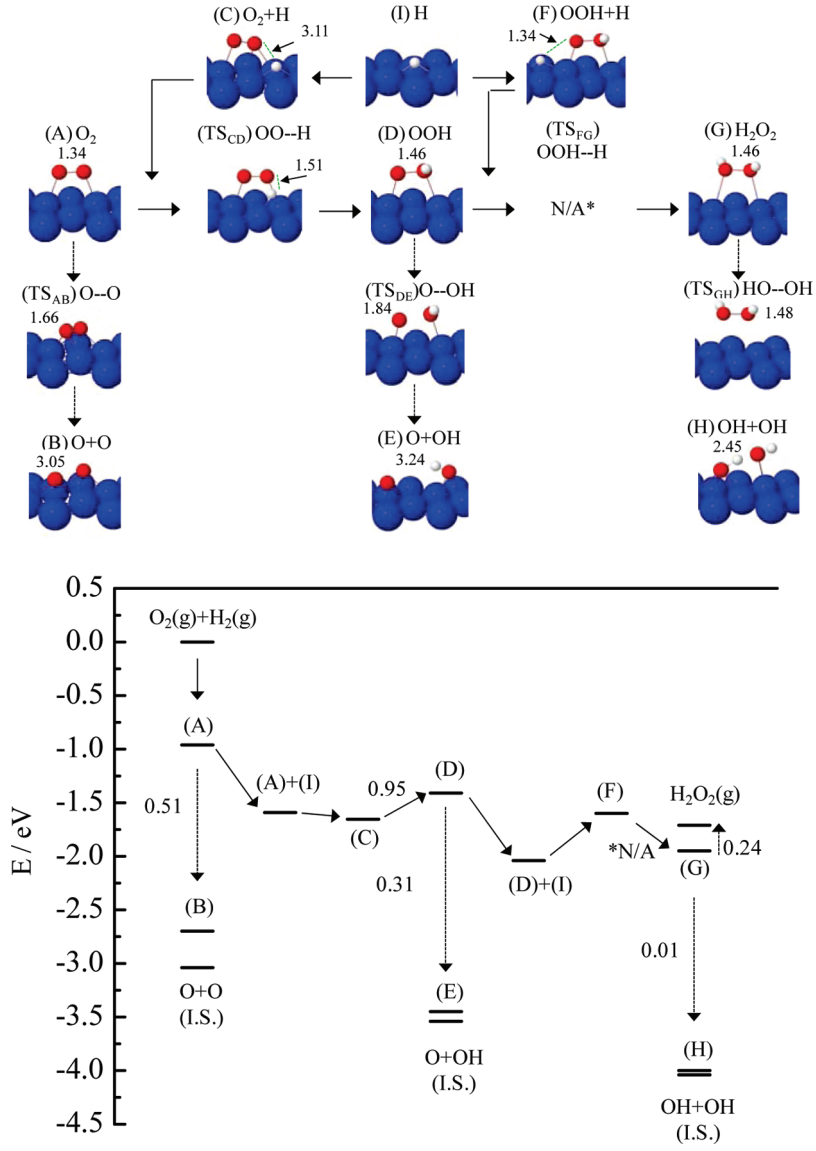


**Figure 4.** Predicted potential energy diagram for direct $H_2O_2$ synthesis from $H_2$ and $O_2$ on pure Pd(111) and corresponding intermediate and transition state configurations. In the energy diagram (lower panel), the activation energies for the hydrogenation, scission, and desorption reactions considered are given in eV, and IS refers to the infinite separation of two adsorbates. On Pt(111), our calculation shows that the hydrogenation of OOH leads to nearly spontaneous dissociation into OH + OH, that is, OOH + H → OH + OH, and thus no activation energy was obtained for the hydrogenation reaction, as indicated by N/A. In the intermediate and transition states, the O−H and O−O distances are indicated in the hydrogen and scission reactions, respectively. The big black (blue), small dark gray (red), and small white balls represent Pd, O, and H atoms, respectively.

**TABLE 2: Calculated Total Energy Changes ($\Delta E$) and Activation Barriers ($E_a$ in Parentheses) for Hydrogenation and Scission Reactions (As Illustrated in Figure 3) with Respect to Fully Separated Coadsorbed Species[a,b]**

| | Pd(111) | $AuPd_M$/Pd(111) | $AuPd_M$/Au(111) | $Au_{41}Pd@Pd_{13}$ |
|---|---|---|---|---|
| $O_2 + H \rightarrow OOH$ (A) | 0.18 (0.89) | −0.73 (0.53) | −0.67 (0.51) | −0.50 (0.72) |
| $O_2 \rightarrow O + O$ (A)′ | −2.08 (0.51) | 0.25 (1.55) | −0.86 (0.93) | −0.37 (0.98) |
| $OOH + H \rightarrow H_2O_2$ (B) | 0.09 (−)[c] | −0.86 (0.37) | −0.71 (0.71) | −0.36 (0.62) |
| $OOH \rightarrow O + OH$ (B)′ | −2.13 (0.31) | −0.39 (0.81) | −1.27 (0.32) | −1.14 (0.45) |
| $H_2O_2 \rightarrow H_2O_2$(g) (C) | 0.24 (0.24) | 0.17 (0.17) | 0.23 (0.23) | 0.40 (0.40) |
| $H_2O_2 \rightarrow OH + OH$ (C)′ | −2.09 (0.01) | −0.90 (0.31) | −1.64 (0.23) | −2.05 (0.17) |

[a] The separation state was evaluated by individually placing each adsorbed species on the $2\sqrt{3} \times 4$ unit surface cell employed in this work. [b] All energy values are given in eV. [c] The OOH hydrogenation results in almost spontaneous HO−OH dissociation with no sizable barrier, that is, $OOH + H \rightarrow OH + OH$.

neighboring Au atoms affects the energetics of $H_2O_2$ formation from $H_2$ and $O_2$. The direct $H_2O_2$ synthesis may predominantly occur via two successive $O_2$ hydrogenation reactions following a Langmuir−Hinshelwood mechanism,[20] as reasoned in our recent paper.[8]

As illustrated in Figure 3, we examined three $H_2O_2$ formation steps and their competing (decomposition) counterparts: $O_2$ hydrogenation [(A)] vs O + O scission [(A)′]; (2) OOH hydrogenation [(B)] vs O + OH scission [(B)′]; and $H_2O_2$ desorption [(C)] vs OH + OH scission [(C)′]. Figures 4−7 show the minimum-energy paths identified for the hydrogenation and dissociation reactions, together with energy variations along the reaction coordinates. For each energy diagram, the total energy prior to $H_2$ and $O_2$ adsorption is set to be zero. In Table 2, we

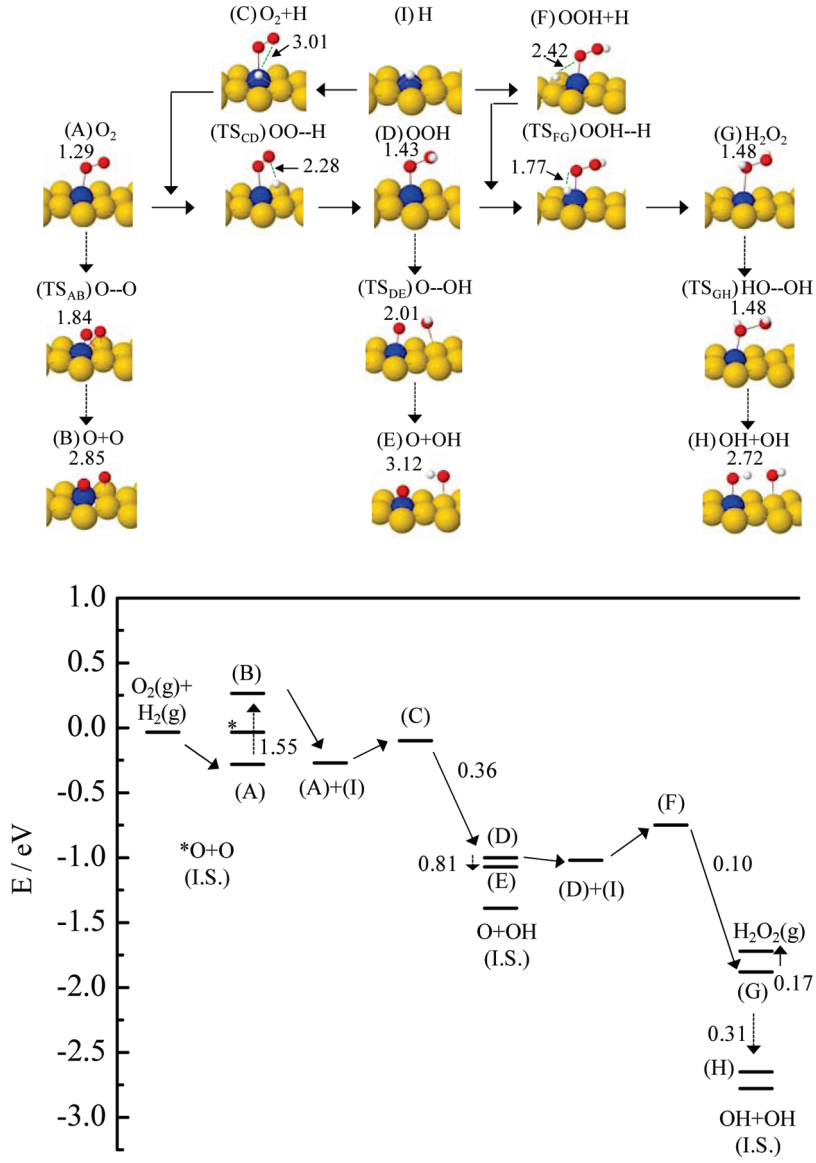


**Figure 5.** Predicted potential energy diagram for direct $H_2O_2$ synthesis from $H_2$ and $O_2$ at the Pd monomer site in $AuPd_M$/Pd(111) and corresponding intermediate and transition state configurations. In the energy diagram (lower panel), the activation energies for the hydrogenation, scission, and desorption reactions considered are given in eV, and IS refers to the infinite separation of two adsorbates. In the intermediate and transition states, the O−H and O−O distances are indicated in the hydrogen and scission reactions, respectively. The big gray (yellow) and black (blue) balls represent surface Au and Pd atoms, respectively, and the small dark gray (red) and white balls indicate O and H atoms, respectively.

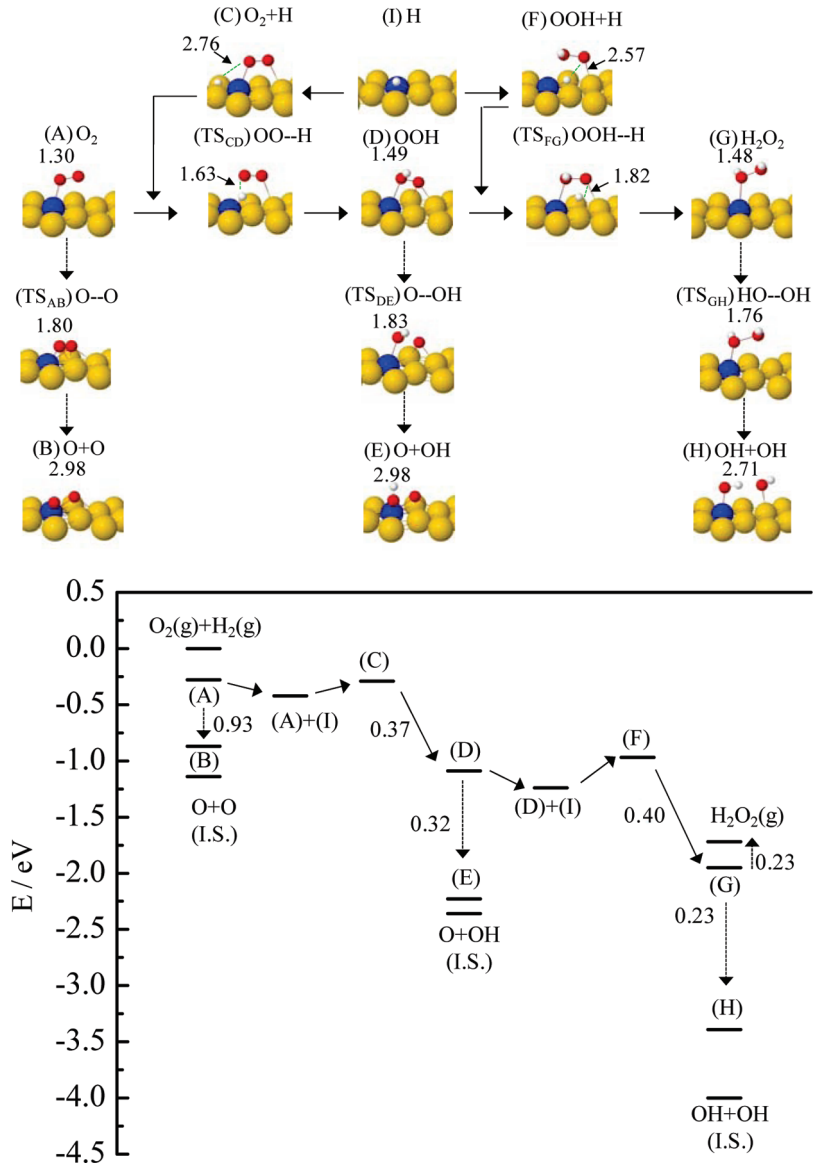


**Figure 6.** Predicted potential energy diagram for direct $H_2O_2$ synthesis from $H_2$ and $O_2$ at the Pd monomer site in $AuPd_M$/Au(111) and corresponding intermediate and transition state configurations. In the energy diagram (lower panel), the activation energies for the hydrogenation, scission, and desorption reactions considered are given in eV, and IS refers to the infinite separation of two adsorbates. In the intermediate and transition states, the O−H and O−O distances are indicated in the hydrogen and scission reactions, respectively. The big gray (yellow) and black (blue) balls represent surface Au and Pd atoms, respectively, and the small dark gray (red) and white balls indicate O and H atoms, respectively.

also summarize the predicted total energy changes ($\Delta E$) and activation barriers ($E_a$), for clarity's sake. The results clearly demonstrate the sensitivity of the reaction energetics and barriers to the change in the Pd and Au electronic states.

On the clean Pd(111) surface [(A) in Figure 4], $O_2$ preferentially adsorbs in an "end-on" configuration where each of the O atoms binds to one of two adjacent Pd surface atoms. The $O_2$ adsorption energy at the top-bridge-top (t-b-t) state is predicted to be 0.95 eV. Here, the adsorption energy ($E_{ad}$) is given by

$$E_{ad} = |E(O_2/M)| - |E(M) + E(O_2)|$$

where $E(O_2/M)$, $E(M)$, and $E(O_2)$ represent the total energies of the $O_2$/slab (or cluster) system, the slab (or cluster), and an isolated $O_2$ molecule in the triplet state, respectively, and $|x|$ indicates the absolute value of $x$. For the $AuPd_M$/Pd(111) case [(A) in Figure 5], one end of O−O binds to the Pd monomer but the other end weakly interacts with an adjacent Au atom, yielding $E_{ad} = 0.25$ eV. The $O_2$ adsorption energy at the t-b-t state increases to 0.27 and 0.75 eV on AuPdM/Au(111) [(A) in Figure 6] and $Au_{41}Pd@Pd_{13}$ [(A) in Figure 7], respectively, yet significantly lower than 0.95 eV for pure Pd(111).

We estimated the atomic charge states of the adsorbed $O_2$ and surface Pd/Au atoms using the Bader method[21] with special care for convergence with respect to charge density grid. The result clearly demonstrates that there is charge transfer from the metal surface to the adsorbed $O_2$; the amount of transferred charge varies from 0.30$e$ [$AuPd_M$/Pd(111)] to 0.34$e$ [$AuPd_M$/Au(111)] and 0.45$e$ [$Au_{41}Pd@Pd_{13}$]. Accordingly, the O−O bond is elongated from 1.24 Å [gas phase] to 1.29 Å [$AuPd_M$/Pd(111)], 1.30 Å [$AuPd_M$/Au(111)], and 1.33 Å [$Au_{41}Pd@Pd_{13}$]. Note that the (transferred) excess charge fills the $O_2$ 2p antibonding orbital, which in turn weakens the O−O bond.

For $O_2$ dissociation, our calculation predicts an endothermicity of 0.25 eV on $AuPd_M$/Pd(111) [(B) in Figure 5]. However, the dissociation reaction turns out to be exothermic by 0.86 and

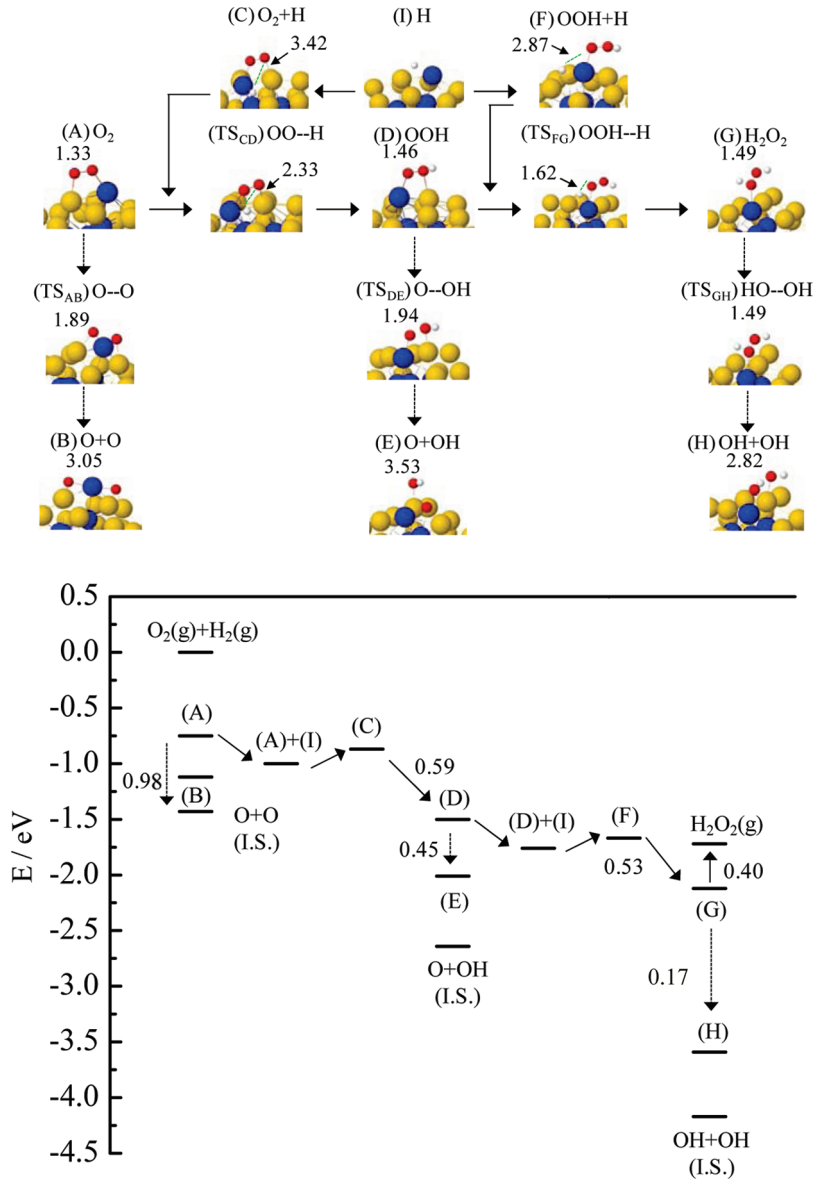


**Figure 7.** Predicted potential energy diagram for direct $H_2O_2$ synthesis from $H_2$ and $O_2$ at the Pd monomer site in $Au_{41}Pd_M@Pd_{13}$ and corresponding intermediate and transition state configurations. In the energy diagram (lower panel), the activation energies for the hydrogenation, scission, and desorption reactions considered are given in eV, and IS refers to the infinite separation of two adsorbates. In the intermediate and transition states, the O−H and O−O distances are indicated in the hydrogen and scission reactions, respectively. The big gray (yellow) and black (blue) balls represent surface Au and Pd atoms, respectively, and the small dark gray (red) and white balls indicate O and H atoms, respectively.

0.37 eV on $AuPd_M/Au(111)$ [(B) in Figure 6] and $Au_{41}Pd@Pd_{13}$ [(B) in Figure 7], respectively. The dissociated O atoms are preferentially located at two fcc sites adjacent to the Pd monomer. The dissociation barrier reduces from 1.55 eV [$AuPd_M/Pd(111)$] to 0.93 eV [$AuPd_M/Pd(111)$] and 0.98 eV [$Au_{41}Pd@Pd_{13}$]. The enhanced reactivity toward $O_2$ unequivocally indicates that the chemical activity of both Pd monomer and Au neighbors is increased. On clean Pd(111), the $O_2$ dissociation is predicted to occur by crossing a barrier of 0.51 eV, with an exothermicity of −2.08 eV.

For $O_2$ hydrogenation, H (in the proximity of $O_2$) is preferentially anchored at a hollow site adjacent to the Pd monomer at the initial state ("coadsorbed"). The coadsorbed state turns out to be less favorable than that the adsorbed H and $O_2$ are fully separated ("at infinite separation"). This indicates that the interaction of $O_2$ and H can be repulsive. Hereafter, the energy required for the coadsorption from the full separation is referred to as the proximity energy. The predicted proximity energies are 0.17, 0.13, and 0.13 eV for $AuPd_M/Pd(111)$, $AuPd_M/Au(111)$, and $Au_{41}Pd@Pd_{13}$, respectively. Including the respective proximity energies, the activation energies for the $O_2$ hydrogenation are estimated to be 0.53, 0.51, and 0.72 eV on $AuPd_M/Pd(111)$, $AuPd_M/Au(111)$, and $Au_{41}Pd@Pd_{13}$, respectively.

For the OOH + H → HOOH and OOH → O + OH reactions, the hydrogenation barrier of 0.37 eV (including the proximity energy of 0.27 eV) is noticeably lower than 0.81 eV for the O−OH bond cleavage on $AuPd_M/Pd(111)$. The O−OH scission barrier decreases to 0.45 and 0.32 eV on $Au_{41}Pd@Pd_{13}$ and $AuPd_M/Au(111)$, respectively, while the hydrogenation barrier increases to 0.62 eV (0.09 eV) and 0.71 eV (0.31 eV); the respective proximity energies included are indicated in parentheses. Expecting that the barrier changes are related to the relative binding strength between OOH and dissociated O/OH radicals, we also compared their binding energies. As summarized in Table 3, the O/OH binding energies noticeably vary

**TABLE 3: Calculated Binding Energies (in eV) of O and OH Radicals**

| | Pd(111) | $AuPd_M$/Pd(111) | $AuPd_M$/Au(111) | $Au_{41}Pd@Pd_{13}$ |
|---|---|---|---|---|
| O | 4.95 | 3.43 | 4.00 | 3.98 |
| OH | 2.67 | 2.01 | 2.30 | 2.67 |

from 3.43/2.01 eV [$AuPd_M$/Pd(111)], 4.00/2.30 eV [$AuPd_M$/Au(111)] to 3.98/2.67 eV [$Au_{41}Pd@Pd_{13}$], while the variation of OOH binding strength is rather insignificant, i.e., 0.89 eV [$AuPd_M$/Pd(111)], 0.98 eV[$AuPd_M$/Au(111)], and 1.39 eV [$Au_{41}Pd@Pd_{13}$]. Our results clearly demonstrate that the enhanced chemical activity of the Pd and neighboring Au atoms leads to facilitating the O−OH bond cleavage, thereby deteriorating the selectivity of $H_2O_2$ formation.

Finally we compared the barriers for $H_2O_2$ desorption vs OH + OH scission. The predicted $H_2O_2$ desorption energies vary from 0.17 eV [$AuPd_M$/Pd(111)], 0.23 eV [$AuPd_M$/Au(111)] to 0.40 eV [$Au_{41}Pd@Pd_{13}$]. The barrier for HO−OH bond scission also noticeably varies, but in the opposite direction, i.e., 0.31 eV [$AuPd_M$/Pd(111)], 0.21 eV [$AuPd_M$/Au(111)], and 0.17 eV [$Au_{41}Pd@Pd_{13}$]. The results clearly demonstrate that the scission barrier can be higher or lower than the desorption barrier depending on the activity of the Pd monomer and its nearest Au neighbors.

Our study clearly demonstrates that the enhanced chemical activity of the Pd and adjacent Au atoms leads to a significant reduction in the scission barriers of adsorbed O−O, O−OH, and HO−OH, while the barriers for $O_2$ adsorption and hydrogenation reactions tend to increase, as summarized in Table 2. As a consequence, the selectivity of $H_2O_2$ formation will be significantly deteriorated in the $Au_{41}Pd@Pd_{13}$ and $AuPd_M$/Au(111) cases as compared to the $AuPd_M$/Pd(111) case. This is consistent with earlier experimental studies[22] that show significant enhancement in catalytic activity toward $H_2O_2$ synthesis as the AuPd particle size increases. The tunability of the reaction energetics suggests the importance of the interplay between surface electronic state alternation (electronic effect) and atomic ordering (geometric effect) in determining preferred reaction routes and activation energies.

## 4. Conclusions

Using first principles DFT calculations, we attempted to examine how the surface reactivity of bimetallic alloys is influenced by the interplay between ensemble and electronic contributions in association with changes in their geometric parameters. We particularly looked at $H_2O_2$ formation from $H_2$ and $O_2$ on three different AuPd alloy surfaces (each of which contains a Pd monomer) modeled using slab and cluster geometries, such as $AuPd_M$/Pd(111), $AuPd_M$/Au(111), and $Au_{41}Pd@Pd_{13}$. The Pd monomer systems were chosen because isolated Pd monomers surrounded by less active Au atoms are likely responsible for promoting $H_2O_2$ formation by suppressing O−O bond cleavage. The ensemble effect is primarily attributed to the large activity difference between Pd and Au, while the direct $H_2O_2$ synthesis may involve two successive $O_2$ hydrogenation reactions and their competing O−O scission reactions. Knowing that, in this work special attention was paid to examining the impact of changes in the electronic states of surface Pd and neighboring Au atoms on the activity and selectivity in the direct $H_2O_2$ synthesis. Our analysis of electronic density of states shows that the activity of a Pd monomer and its Au neighbors can substantially vary with geometric conditions; among those three model systems considered the highest activity occurs in $Au_{41}Pd@Pd_{13}$, followed by $AuPd_M$/Au(111) and $AuPd_M$/Pd(111). The activity enhancement of the skin surface Pd and Au atoms is associated with their reduced coordination number and inherent mechanical strain created in the small cluster. Likewise, the $AuPd_M$/Au(111) case is mainly attributed to the tensily strained Pd site where the Pd−Au distance is increased to 2.93 Å, as compared to 2.78 Å for the $AuPd_M$/Pd(111) case. The enhanced chemical activity of the Pd and adjacent Au atoms leads to significant deterioration in the selectivity of $H_2O_2$ formation by decreasing the scission barriers of adsorbed O−O, O−OH, and HO−OH, while the barriers for $O_2$ adsorption and hydrogenation reactions tend to increase. Our study highlights that the ensemble effect on the performance of alloy catalysts is subject to surface electronic states that can be greatly altered by the change of catalyst's geometric parameters, particularly related to local strain and effective atomic coordination number at the surface. This might warrant further investigations to the effects of catalyst geometry on the arrangement and activity of surface atoms, which will allow a better understanding of the interplay between ensemble and electronic contributions that are necessary for rationally designing multimetallic nanocatalysts.

**Acknowledgment.** This work was supported by the R.A. Welch Foundation (F-1535). The authors also thank the Texas Advanced Computing Center for use of their computing resources.

**Supporting Information Available:** Figure S1. This material is available free of charge via the Internet at http://pubs.acs.org.

## References and Notes

(1) Edwards, J. K.; Carley, A. F.; Herzing, A. A.; Kiely, C. J.; Hutchings, G. J. *Faraday Discuss.* **2008**, *138*, 225.
(2) Abate, S.; Centi, G.; Melada, S.; Perathoner, S.; Pinna, F.; Strukul, G. *Catal. Today* **2005**, *104*, 323.
(3) Allison, E. G.; Bond, G. C. *Catal. Rev.* **1972**, *7*, 233.
(4) Chen, M. S.; Kumar, D.; Yi, C. W.; Goodman, D. W. *Science* **2005**, *310*, 291.
(5) Yi, C. W.; Luo, K.; Wei, T.; Goodman, D. W. *J. Phys. Chem. B* **2005**, *109*, 18535.
(6) Maroun, F.; Ozanam, F.; Magnussen, O. M.; Behm, R. J. *Science* **2001**, *293*, 1811.
(7) Liu, P.; Norskov, J. K. *Phys. Chem. Chem. Phys.* **2001**, *3*, 3814.
(8) Ham, H. C.; Hwang, G. S.; Han, J.; Nam, S. W.; Lim, T. H. *J. Phys. Chem. C* **2009**, *113*, 12943.
(9) Pluntke, Y.; Kibler, L. A.; Kolb, D. M. *Phys. Chem. Chem. Phys.* **2008**, *10*, 3684.
(10) Perdew, J. P.; Wang, Y. *Phys. Rev. B* **1992**, *45*, 13244.
(11) Kresse, G.; Furthmuller, J. *VASP the Guide*; Vienna University of Technology: Vienna, Austria, 2001.
(12) Blochl, P. E. *Phys. Rev. B* **1994**, *50*, 17953.
(13) Henkelman, G.; Uberuaga, B. P.; Jonsson, H. *J. Chem. Phys.* **2000**, *113*, 9901.
(14) Eichler, A.; Mittendorfer, F.; Hafner, J. *Phys. Rev. B* **2000**, *62*, 4744.
(15) Roudgar, A.; Gross, A. *Surf. Sci.* **2004**, *559*, L180.
(16) Ruban, A.; Hammer, B.; Stoltze, P.; Skriver, H. L.; Norskov, J. K. *J. Mol. Catal A: Chem.* **1997**, *115*, 421.
(17) Kitchin, J. R.; Norskov, J. K.; Barteau, M. A.; Chen, J. G. *J. Chem. Phys.* **2004**, *120*, 10240.
(18) Mavrikakis, M.; Hammer, B.; Norskov, J. K. *Phys. Rev. Lett.* **1998**, *81*, 2819.
(19) Schlapka, A.; Lischka, M.; Gross, A.; Kasberger, U.; Jakob, P. *Phys. Rev. Lett.* **2003**, *91*.
(20) Edwin, N. N.; Edwards, J. K.; Carley, A. F.; Lopez-Sanchez, J. A.; Moulijn, J. A.; Herzing, A. A.; Kiely, C. J.; Hutchings, G. J. *Green Chem.* **2008**, *10*, 1162.
(21) Sanville, E.; Kenny, S. D.; Smith, R.; Henkelman, G. *J. Comput. Chem.* **2007**, *28*, 899.
(22) Solsona, B. E.; Edwards, J. K.; Landon, P.; Carley, A. F.; Herzing, A.; Kiely, C. J.; Hutchings, G. J. *Chem. Mater.* **2006**, *18*, 2689.

JP102851D